Journal of Marine Research, 50, 611–642, 1992

Numerical modeling of larval settlement in turbulent bottom boundary layers

by Thomas F. Gross[1], Francisco E. Werner[1] and James E. Eckman[1]

ABSTRACT

A time-dependent model of a tidal or wave bottom boundary layer has been developed to quantitatively evaluate the relative influences of vertical advection, turbulent mixing and shear, and near-bed behavior on settlement of planktonic larvae of benthic animals. The settlement behavior of larvae is modeled with a simple flux condition at the bed. This allows full time dependence to be included when determining settlement rates. For tidal oscillations, the model predicts that most settlement will occur at and near periods of slack water, whereas comparatively little settlement will occur during periods of stronger flow. In contrast, there should be little temporal variability in settlement rates associated with short-period wind waves. If larvae exhibit a relatively weak propensity to settle, then the settlement flux is small compared to the advective/turbulent flux of larvae supplied from higher in the water column to regions near the bed. In this case, a description of probability of settlement and a quasi-steady state suspension model fully describe the system. In contrast, when larvae exhibit a high settlement propensity, then the settlement flux is potentially larger than the advective/turbulent flux and the system is controlled by the hydrodynamic supply of larvae to the near-bed region. In this case, net settlement is governed primarily by larval fall velocity (a composite of gravitational sinking plus swimming) and turbulent shear stress. The ecological systems which are controlled by animal behavior or by physical processes may thus be identified by estimates of relatively simple parameters describing these fluxes.

1. Introduction

The recruitment of benthic invertebrates is highly variable in space and time. This variability has long been appreciated, and has been attributed, in part, to patterns of oceanic and local circulation (e.g., Ekman, 1967; Scheltema, 1974; Shanks, 1986; Shanks and Wright, 1987; Roughgarden *et al.,* 1988; Wolanski and Hamner, 1988), to differential selectivity of substrata by larvae (e.g., Meadows and Campbell, 1972; Gray, 1974; Crisp, 1984; Woodin, 1986), and to post-settlement events that affect mortality (e.g., Connell and Slatyer, 1977; Paine, 1979; Keough and Downes, 1982; Summerson and Peterson, 1984; Peterson, 1986; Fairweather, 1988). Prior research has greatly expanded our understanding of the diverse factors that affect recruitment and the extent to which these factors may operate. However, with few exceptions

1. Skidaway Institute of Oceanography, P. O. Box 13687, Savannah, Georgia, 31416, U.S.A.

(e.g., Roughgarden *et al.*, 1988; Eckman, 1990; Pineda, 1991), past research has left marine ecologists with an inadequate capability to predict quantitatively the extent to which larval settlement and recruitment may vary in space and time.

Simple scaling arguments (e.g., Butman, 1986) indicate that most planktonic larvae are dispersed horizontally by currents in an essentially passive manner, with most larvae capable of exerting control over no more than their vertical position in the water column (e.g., Grosberg, 1982). Thus, hydrodynamic processes affect intensities of larval settlement over both large and small spatial and temporal scales (e.g., Eckman, 1983; 1987; 1990; Jackson, 1986; Wethey, 1986; Butman *et al.*, 1988; Roughgarden *et al.*, 1988; Wolanski and Hamner, 1988). However, the sophisticated selective capacities of many larvae (e.g., see reviews by Crisp, 1984; Woodin, 1986) indicate that behavior also plays an important role in determining ultimate sites of settlement. Thus, settlement is subject to both hydrodynamic and behavioral controls. Our capacity to understand and predict the variability of larval settlement in space and time depends on developing a quantitative understanding of the relative roles of transport processes and larval behavior in delivering larvae to potential settlement sites, and flow forces, larval development and larval behavior in determining probabilities of settlement after a potential settlement site is contacted. An integrated, quantitative understanding of these aspects of recruitment dynamics has yet to be developed, and is the ultimate goal driving our initial modeling efforts described herein.

Toward that end a time-dependent model of a tidal or wave bottom boundary layer has been developed to quantitatively evaluate the relative influences of vertical advection, turbulent mixing and shear, and boundary processes upon settlement of planktonic larvae of benthic animals. Planktonic larvae of benthic invertebrates settle through a turbulent boundary layer to the bottom which they sense, evaluate and may explore before undergoing permanent metamorphosis. The supply of larvae to the near-bed region will be controlled by vertical advection (e.g., gravitational sinking), turbulent mixing and vertical swimming. The rate of attachment to the bed will be controlled by the number of larvae interacting with the bed, and their predilection toward settlement. It is the goal of this paper to examine the effects of hydrodynamic processes within the turbulent boundary layer on settlement rate, and to indicate the extent to which hydrodynamic controls on settlement rate may be mediated or overridden by larval behavior. A boundary layer model in which behavioral parameters are treated simply will be used to examine the hydrodynamic side of the problem. We focus, in particular, on evaluating the effects of time dependence within wave or tidally forced flows, because steady models of turbulent boundary layers may not address these dominant features of natural oceanic flows adequately (e.g., Grant and Madsen, 1986).

In classical advection-diffusion models of suspended particle transport the hydrodynamic control of suspended particles is provided by specification of an advection

velocity (the gravitational fall velocity) and the turbulent eddy diffusivity (e.g., Sheng and Lick, 1979; Middleton and Southard, 1984). The 1-D profile model of suspended particle transport can be applied successfully to horizontally uniform flows (Gross and Dade, 1991). To apply suspended particle modeling techniques we define larvae by a single, constant vertical fall velocity which represents the composite of gravitational sinking and an assumed invariant swimming vector. Several turbulence closure methods are available which give different levels of approximation to the "true" diffusivity. The turbulent kinetic energy closure method resolves temporal and spatial variability expected in shallow or strongly forced wave environments. This method is used here and has been used to model the flow field under gravity waves with frequencies from tidal/inertial to wind waves (Bradshaw *et al.,* 1967; Davies, 1986; Mofjeld and Lavelle, 1984; Gross and Nowell, 1990; Gross and Dade, 1991; Davies and Jones, 1991).

The rate of larval settlement to the bottom is the primary focus of this study. Towards this end we impose a bottom boundary condition in terms of larval flux to the bed. The total settlement flux of larvae is specified as the product of the number of larvae (per area of bottom) interacting with the bottom (i.e., available for settling) and their probability of settlement. We have incorporated all aspects of larval response to the substratum in terms of this simple probability statement.

We next describe the formulation of our model of time-dependent momentum, turbulent kinetic energy, and larval concentration in the water column (Section 2), followed by an evaluation of the turbulent kinetic energy method of specifying eddy diffusivities, relative to simpler parameterizations (Section 3). Readers who are less interested in the details of our mathematical treatment may wish to skim Sections 2 and 3. Thereafter, we detail our boundary condition that predicts larval settlement rate (Section 4), followed by a dimensional analysis of both water-column and boundary processes (Section 5). Model results are then described (Section 6) and put into perspective (Section 7).

2. Model formulation

We solve for the time-dependent vertical distribution of a concentration of larvae in a one-dimensional turbulent boundary layer. Coupled momentum and turbulent kinetic energy equations define the hydrodynamic setting (e.g., Bradshaw *et al.,* 1967; Rodi, 1984; Mofjeld and Lavelle, 1984; Davies *et al.,* 1988). Through mixing length parameterization (e.g. Blackadar, 1962), a vertical eddy viscosity is computed which, in conjunction with an externally imposed vertical fall velocity, casts the distribution of larvae in terms of an advection-diffusion equation. An externally imposed fall velocity advects larvae toward the bottom while the turbulence resuspends and redistributes the larvae within the model domain.

a. Concentration and momentum equations. The one-dimensional equation for the distribution of a concentration C of larvae is

$$\frac{\partial C}{\partial t} + \frac{\partial (w_f C)}{\partial z} = \frac{\partial}{\partial z}\left[A_v \frac{\partial C}{\partial z}\right] \tag{1}$$

where the vertical axis is z (positive upward), time is t, w_f is larval fall velocity and A_v is eddy diffusivity. The top boundary condition, $z = h$, is no flux

$$A_v \frac{\partial C}{\partial z} - w_f C = 0. \tag{2}$$

The bottom boundary condition specifying the settlement/resuspension flux will be discussed in Section 4 and Appendix A.

Solution of the suspended larval concentration equation requires specification of the vertical eddy diffusivity A_v. The spatial structure and the time-history of A_v is determined from the momentum and energy equations for a one-dimensional turbulent bottom boundary layer. The equations for the u and v velocity components in a rotating frame are

$$\frac{\partial u}{\partial t} - fv = -\frac{1}{\rho}\frac{\partial P}{\partial x} + \frac{\partial}{\partial z}\left[A_v \frac{\partial u}{\partial z}\right] \tag{3}$$

$$\frac{\partial v}{\partial t} + fu = -\frac{1}{\rho}\frac{\partial P}{\partial y} + \frac{\partial}{\partial z}\left[A_v \frac{\partial v}{\partial z}\right] \tag{4}$$

where ρ is the density, P is the pressure and f is the Coriolis parameter. We have assumed that, except for the pressure gradient term, horizontal gradients (in x and y) may be neglected relative to vertical gradients. Similarly, we have assumed that the (conventional Boussinesq) fluid is of homogeneous density. For simplicity we will from here on restrict our attention to cases where Coriolis may be ignored, e.g. tidal channels or shallow coastal areas. Lastly, we have ignored molecular viscosity and parameterized tangential stresses through an eddy viscosity formulation.

To solve for u and v, we require no-slip at $z = z_o$ (the bottom)

$$u = v = 0 \tag{5}$$

where z_o, the roughness length, represents a small distance above the true bed. Flow over a smooth surface will have a small roughness scale due to the thickness of the viscous layer, $z_o = \nu/9u_*$. Hydraulically smooth surfaces are rare in marine settings and therefore we use the hydraulically rough flow parameterization. In hydraulically rough flow z_o represents the effect of geometric roughness variation upon the turbulent momentum transfer to the ultimately viscous flow layer on, over and around the bed roughness elements. Hydraulically rough flow over sand grains of diameter k_b has $z_o \approx k_b/30$ (Nikuradse, 1933). Similar expressions exist for many

types of regular or irregular roughness which can be characterized by a length scale, k_b (Smith, 1977; Grant and Madsen, 1982; 1986). At the top, $z = h$, we specify the surface velocity

$$u(h, t) = u_h(t), \qquad v(h, t) = v_h(t) \tag{6}$$

and treat the pressure term as described in Appendix B.

We use an eddy viscosity closure which is a function of the turbulent kinetic energy (TKE)

$$A_v = C_a l \bar{k}_e^{1/2} \tag{7}$$

where C_a is a constant, l is the mixing length and $\bar{k}_e$ is the turbulent kinetic energy.

b. Turbulent kinetic energy. The equation for the turbulent kinetic energy $\bar{k}_e$ relates the time rate of change of $\bar{k}_e$ to a production term, a vertical redistribution term and a dissipation term as

$$\frac{\partial \bar{k}_e}{\partial t} = A_v \left\{ \left[\frac{\partial u}{\partial z} \right]^2 + \left[\frac{\partial v}{\partial z} \right]^2 \right\} + \frac{\partial}{\partial z} \left[A_e \frac{\partial \bar{k}_e}{\partial z} \right] - \epsilon \tag{8}$$

where we require no flux at $z = z_o$ and at $z = h$

$$\frac{\partial \bar{k}_e}{\partial z} = 0. \tag{9}$$

The turbulent kinetic energy diffusion is given by

$$A_e = C_e A_v \tag{10}$$

and the dissipation term is parameterized as

$$\epsilon = C_\epsilon \frac{\bar{k}_e^{3/2}}{l}. \tag{11}$$

We use the parametric form of the mixing length, l, given by Blackadar (1962)

$$l(z) = \frac{\kappa z}{\left(1 + \frac{\kappa z}{l_o}\right)}; \qquad l_o = \gamma \frac{\int_{z_o}^{h} z \bar{k}_e^{1/2} dz}{\int_{z_o}^{h} \bar{k}_e^{1/2} dz}. \tag{12}$$

The nondimensional constants are $\kappa = 0.4$, $C_a = 0.5$, $C_e = 0.73$, $C_\epsilon = 0.125$ ($C_\epsilon = C_a^3$) and $\gamma = 0.4$ (Blackadar, 1962). Mofjeld and Lavelle (1984) have examined the effect of the coefficient γ on the boundary layer solution and conclude that near the bed it is not a critical parameter. However the outer part of the boundary layer is affected as the depth of maximum eddy diffusivity is proportional to γ. We err on the

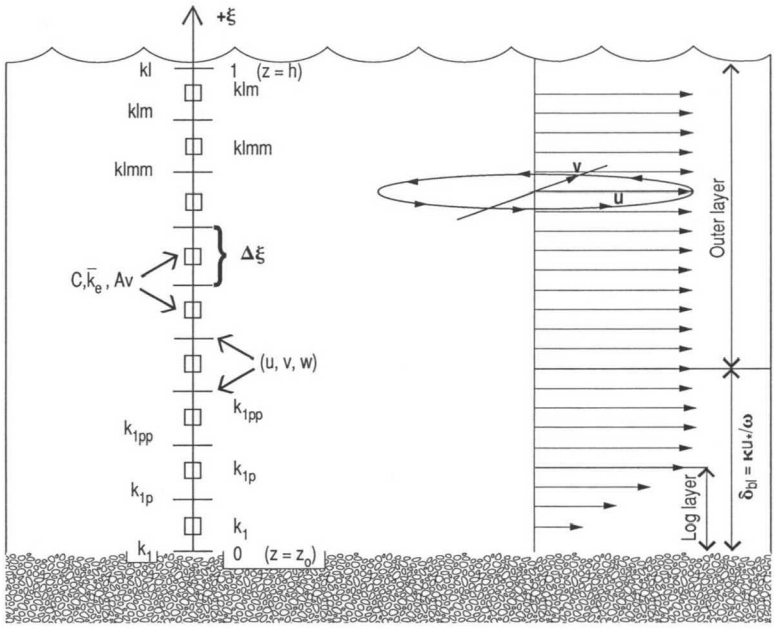

Figure 1. Definition of mesh and model domain. Velocities are staggered relative to the kinetic energy, eddy viscosity and concentration. In the log-linear transformed domain, the grid spacing is constant. A point velocity profile is shown and the logarithmic region, the boundary layer thickness and the free-stream regions are indicated.

side of a large γ, or thicker boundary layer. Quantitative differences in boundary layer thickness due to different values of γ could be absorbed in the definition of boundary layer thickness, i.e. $\delta_{bl} = u_*/\omega$ or $\kappa u_*/\omega$ or $\alpha u_* T$.

c. Numerical considerations and discretization. The numerical treatment of the momentum and TKE equations follows closely that of Ozer *et al.* (1988) and Davies and Jones (1991). The discretization scheme uses 2nd order centered differencing for the interior and the boundaries, with variables staggered as in Figure 1. A banded matrix solution is required at each step for velocity, turbulent kinetic energy and concentration—tridiagonal for the interior points and appropriately modified at the boundaries. The treatment of the pressure gradient term when specifying the free-stream velocity is detailed in Appendix B.

The procedure per time-step is to first solve for velocity, followed by a solution for the turbulent kinetic energy. Using the mixing length equation (Eq. 12) we compute the vertical eddy viscosity profile for that particular time-step. The concentration equation is then advanced in time with updated A_v values. The computation is repeated in the next time step.

Initially the values of velocity are set to zero. The initial turbulent kinetic energy and the eddy viscosity are set to non-zero values: $\bar{k}_e \approx 10^{-4}\text{m}^2\,\text{s}^{-2}$ and $A_v \approx \kappa z \bar{k}_e^{1/2}$.

The concentration profile is set by a steady Rouse profile (see Eq. 19 below). The hydrodynamic component of the model is allowed to "spin-up" for 3 periods before marching forward with the solution of the concentration profile. The concentration profile is allowed to spin up for ten additional periods before solutions are examined. After the spin up phase, transients from the initial values are no longer observed.

3. Time dependent TKE closure versus simple eddy diffusivity

In this section we compare the solutions obtained with TKE closure (Section 2) to those obtained with simpler, externally specified closures. Although most simple eddy diffusivities give similar velocity profiles near the bed, large differences in the suspended particle load distribution with height will be demonstrated. The simple closures obtain the turbulent boundary friction velocity scale, u_*, from the outer forcing velocity, U_h, through drag coefficients, C_d. The simplest of these other closures use eddy diffusivities of constant, linear or mixed formulations (Soulsby, 1990):

$$\begin{array}{lll} \text{Constant} & A_v(z,t) = C_d U_h(t) & \\ \text{Linear} & A_v(z,t) = \kappa z\sqrt{C_d}U_h(t) & \\ \text{Mixed} & A_v(z,t) = \kappa z\sqrt{C_d}U_h(t) & z < Z_{\delta_{bl}} \\ & A_v(z,t) = \kappa Z_{\delta_{bl}}\sqrt{C_d}U_h(t) & z > Z_{\delta_{bl}}. \end{array} \tag{13}$$

Sample runs of the model for a tidal flow with moderate fall velocities are shown in Figure 2 for the three simple eddy diffusivities and the TKE method. The parameters used are listed in Table 1 (row 8). The plot of concentration times z versus logarithm of z preserves area as an indicator of total concentration. The plot resolves the relative contribution of near-bed to outer-bed regions by scaling concentration so that area under the logarithmically stretched z coordinate is directly proportional to larval abundance. The TKE example (Fig. 2d) shows that much of the larval density oscillates up and down close to the bed, due to time variable diffusivity.

The simplest constant eddy diffusivity gives very poor results near the bed, but models the outer region adequately. The concentration profile shows the near bed region is too intensively stirred, with almost no larvae within 20 cm of the bed. The linear diffusivity profile resolves the bottom well, because the form of $\kappa z u_*$ is compatible with the known asymptotic "inner layer" boundary layer solution. But because the linear diffusivity increases up to the surface the outer region is overly stirred and too many larvae are suspended in the upper region. Unlike the constant diffusivity case, there is some larval concentration near the bed, but the magnitude is low because much of the larvae are kept in suspension higher in the water column. The mixed method matches the best of both forms to give the proper asymptotic limits in both inner and outer regions. The point at which they are joined, $Z_{\delta_{bl}}$, is externally specified in this case. It can be seen that further refinements are possible

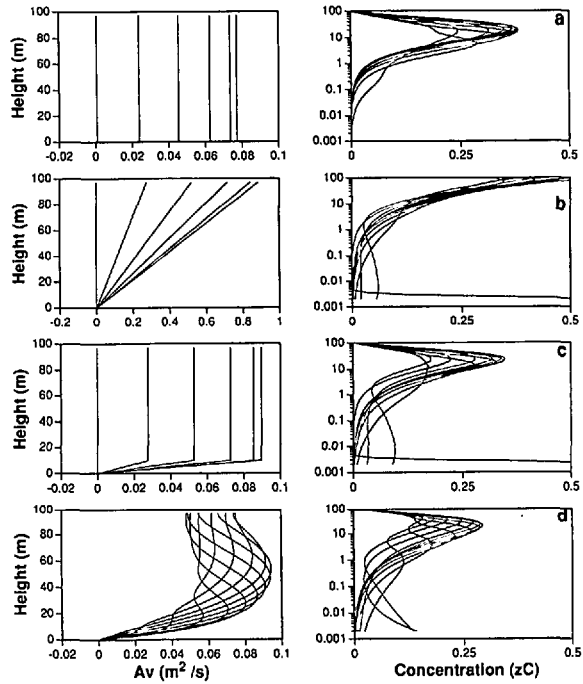

Figure 2. Eddy diffusivity, and concentration profiles over time during a tidal oscillation for the case of (a) constant, (b) linear, (c) mixed constant and linear eddy diffusivities and (d) the case using the turbulent kinetic energy closure. The concentration plots are scaled by multiplying by z. This creates a log-linear plot where area under the $zC(z)$ curve is proportional to total mass in suspension.

by introducing additional *ad hoc* parameters such as $Z_{\delta_{bl}}$ to describe features such as boundary layer thickness, phase shifts between outer velocity, inner velocity and eddy diffusivity and minimal turbulence levels. Most of these features are natural results of the TKE formulation.

The drag-coefficient forms of eddy diffusivity create several unrealistic features. Foremost is that during an oscillating flow the drag coefficient formulation allows the diffusivity to become zero at slack water causing an unrealistic increase of the near bed concentration. This does not occur in nature (except under conditions of extreme weak forcing). The concentration profile equation becomes almost purely hyperbolic giving rise to numerical difficulties under the solution scheme used here. We imposed a minimum level of diffusivity (10^{-3}m^2 s^{-1} for the constant case and $\nu = 1.5 \times 10^{-6}$m^2 s^{-1} for the linear case). The very low diffusivity around slack water is much less than the minimum of the TKE closure. Differences among the closure schemes greatly affect changes in the maximum concentration near the bed. The discrepancy needs to be resolved with laboratory observations as it can be quite significant to predicting settlement rates.

Table 1. Parameters of cases used in figures. All units are in meters and seconds. A constant value of $z_o = 0.002$ m was used for all cases.

	Case	Depth h	Period T	U_h	w_f	w_s	u_{*max}	h/z_o	δ_{bl}/h	$w_f/\kappa u_*$	w_s/w_f
1	Tide	100	21600	0.21	0.0008	—	0.01	50000	0.14	0.18	—
2	Tide	100	21600	0.21	0.0015	—	0.01	50000	0.14	0.37	—
3	Tide	100	21600	0.21	0.0030	—	0.01	50000	0.14	0.74	—
4	Tide	100	43200	0.24	0.0008	—	0.01	50000	0.28	0.18	—
5	Tide	100	43200	0.24	0.0015	—	0.01	50000	0.28	0.37	—
6	Tide	100	43200	0.24	0.0030	—	0.01	50000	0.28	0.74	—
7	Tide	100	43200	0.52	0.0015	—	0.02	50000	0.55	0.19	—
8	Tide	100	43200	0.52	0.0030	—	0.02	50000	0.55	0.37	—
9	Tide	100	43200	0.52	0.0060	—	0.02	50000	0.55	0.75	—
10	Tide	100	86400	1.13	0.0030	—	0.04	50000	2.19	0.19	—
11	Tide	100	86400	1.13	0.0060	—	0.04	50000	2.19	0.38	—
12	Tide	100	86400	1.13	0.0120	—	0.04	50000	2.19	0.75	—
13	Wave	10	20	0.28	0.0030	—	0.04	5000	0.01	0.19	—
14	Wave	10	20	0.28	0.0060	—	0.04	5000	0.01	0.38	—
15	Wave	10	20	0.28	0.0120	—	0.04	5000	0.01	0.76	—
16	Settle	100	43200	0.52	0.0030	0.000003	0.02	50000	0.55	0.37	0.001
17	Settle	100	43200	0.52	0.0030	0.000003	0.02	50000	0.55	0.37	0.010
18	Settle	100	43200	0.52	0.0030	0.000003	0.02	50000	0.55	0.37	0.100

The TKE closure shows considerable phase shift in A_v from top to bottom, with the point of maximum diffusivity moving up and down through the wave cycle. The simple drag coefficient formulations lack this phase shift. The phase differences are evident in the diffusivity profiles but do not strongly affect the mean velocity profile. This characteristic has allowed successful modeling of velocity profiles with drag coefficients. However the larval distribution profiles are qualitatively affected by these differences in diffusivity. Part of the complicated time dependent structure near the bed is created by the time lag of falling larvae relative to the changing diffusivity. These interactions cannot be modeled accurately with the drag coefficient formulation.

4. Boundary conditions for settlement and resuspension

Larval settlement is assumed to be driven, in part, by the near-bed supply of larvae from the overlying water column (cf., Eckman, 1990). Thus, the bed settlement flux will be assumed to be concentration specific and, additionally, a function of processes operating at the bed including animal behavior, hydrodynamic forcing and the physical properties of the bed. That is, the settlement flux is always directly proportional to the supplied concentration specified just above the bed. In this manner the two major components of the system, the model of the temporal and

spatial variability of the concentration distribution in the water column, and the model of larval settlement flux, may be decoupled.

Suspended sediment models have often specified the bottom boundary condition by modeling an underlying bedload or saltation layer. A model of bedload dynamics is used to predict the height of the bedload layer and the concentration of saltating particles at that height (e.g. Smith and McLean, 1977; Wiberg, 1988; Wiberg and Smith, 1989). This concentration is then taken as the bottom condition for the overlying suspended sediment model. This technique is appropriate for suspended sediment whose source is the bed and for which a dynamic bed load model may be devised. However, larvae do not interact with the bed only as ballistic particles and another approach to the boundary condition is necessary for this and additional reasons. First, a population of larvae which have developed to a competent stage have been in the water column for hours or days. These larvae do not have a local or continuous source at the bed. Second, larval selection or rejection of the bed is not dictated by probability of ejection by saltation motion. Selection can be viewed as an interaction with the bed which results in either attachment or rejection back to the suspended flow. The depth of the interaction layer will not be determined by a balance of gravity and ballistic trajectories, as is the case with sediments, but rather will be a function of the size and sensory capacities of the larvae, and perhaps the turbulence strength (see below). Moreover, larvae may actively swim away from the bed when rejecting it rather than simply rolling away along the bottom (e.g., Butman *et al.,* 1988; Pawlik *et al.,* 1991).

A dynamic flux condition allows full time dependence in the boundary condition and concentration term. The total flux at the bed is a combination of the flux due to fall velocity and turbulent eddy diffusion and that due to the settlement/erosion flux

$$\Phi = w_f C - A_v \frac{\partial C}{\partial z} - (w_s C + w_e C_{bed}) \tag{14}$$

where w_s scales the concentration-specific settlement flux. w_e and C_{bed} are erosion parameters which would describe bed erosion flux in a suspended sediment model (or spawning, in a larval model). In the cases considered here the resuspension/erosion flux is set to zero. Finally, with this flux boundary condition, the near-bed time rate of change of concentration at z is

$$\left.\frac{\partial C}{\partial t}\right|_z = \left.\frac{\partial \Phi}{\partial z}\right|_z . \tag{15}$$

An alternative form of the settlement flux, $\Phi_S = w_s C$, can be posed indicating how the behavior of larvae can impact the settlement flux. The bed settlement flux can be specified in terms of the probability per unit time, p, that N larvae per area will settle. This is apparently a more convenient statement of flux to be measured in the laboratory. However the transference of number per area to number per volume

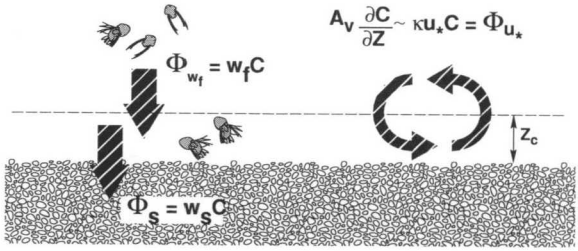

Figure 3. The net flux of larvae into (and out of) the near-bed region over the distance z_c results from the combination of three distinct flux terms: Φ_{w_f} is the flux from above due to fall velocity; Φ_{u_*} is the flux due to turbulent diffusion (which can be into the near-bed region if the flux is from above z_c or out of the near-bed region if the larvae within z_c are being resuspended); and, Φ_s is the flux out of the z_c region to the bed through the larvae's permanent attachment or settlement.

requires the specification of an interaction distance, z_c. This is the distance in which a larva is close enough to the bed to interact with the bed, sense and finally attach to the bed. The settlement flux can be expressed both ways,

$$\Phi_S = pN = pz_cC = w_sC \tag{16}$$

where C is here the average concentration of larvae below z_c. The interaction probability per time (p) is applied to all individuals within the interaction distance. An experiment which measures p and N either implicitly assumes an interaction distance or does not model the transition from suspension to the bed, i.e. all the larvae begin in contact with the bed and a probability of attachment or metamorphosis is measured.

The probability of attachment, and the interaction distance z_c, must be derived from experimental observations of the behavior of settling larvae. In this paper we simply parameterize their product as the settling velocity, w_s. This allows evaluation of the range of values of w_s for which it controls the larval settlement rate. It will be shown that the flux of larvae to the bed can be controlled either by the settling velocity or by the hydrodynamic flux of larvae from higher in the water column to the near-bed region due to advection (larval fall velocity) and turbulent diffusion. The near-bed fluxes within the interaction distance z_c are diagrammed in Figure 3.

Larvae above the interaction distance, z_c, are assumed to have a zero probability of settlement. Therefore it is of fundamental importance to determine the number of larvae below z_c and how this number varies as a function of time. In a no-settlement case ($p = 0$) the concentration of larvae below z_c may reveal the times of potentially maximum settlement rate. Therefore, even though the settlement model requires only w_s, specification of z_c can be quite informative.

Two simple methods of specifying z_c can be used. First, it is taken to be a simple geometric scale related to the size of a larva or the distance over which it can sense its surroundings. We have chosen a multiple of the bed roughness ($3\,k_b$ or $90\,z_o$) which

we assume scales to the approximate size of a typical larvae (0.1 – 1 mm). Alternatively, z_c may depend on the temporal pattern of turbulence near the bed. In an extension of Dade *et al.*'s (1988) model of fine-particle contact with the bed, here it is assumed that larvae can contact the bed only within the "quiet" interval between intense bursts of turbulence that characterize the sediment-water interface (e.g. Cantwell, 1981; Dade *et al.*, 1988; Gross and Dade, 1991). In hydrodynamically smooth flow the quiet period, t_q, scales as $40\,\nu/u_*^2$ (Bandyopadhyay, 1987). Alternatively, use of an outer scaling in hydrodynamically rough flow, produces a similar relationship, $t_q \approx 6\delta_{bl}/U_h$, where δ_{bl} is boundary layer depth and U_h is mean outer velocity (Cantwell, 1981). Thus, larvae closer to the bed than $w_f t_q$ should be able to contact the bed within one quiet period. This distance is:

$$z_c = 40 w_f \nu / u_*^2. \tag{17}$$

More study of the form and dependence of z_c on flow parameters and based in experiment are necessary. Here a simple u_* dependent form for z_c is presented to illustrate the possible effect of time dependence of z_c upon total settlement rates.

We apply one final condition to our parameterization of settlement flux. Just as inorganic sediment has critical stress thresholds for erosion and redeposition, we expect that larvae will not settle when the bed stress exceeds some critical shear stress, τ_c, in part because of the mechanical damage potentially suffered by soft-bodied organisms that would settle among jostling grains. Thus, the probability of settlement varies as a function of bed stress. The functional dependence of w_s on τ is unknown for any species. For illustration we set the settlement velocity to zero whenever a specified critical stress threshold is exceeded

$$\begin{aligned} w_s &= 0 \qquad \tau > \tau_c \\ w_s &= pz_c \qquad \tau < \tau_c \,. \end{aligned} \tag{18}$$

We will use $\tau_c \approx 0.1\tau_{max}$ to illustrate the time dependence of settlement as affected by τ_c.

5. Dimensional analysis

There appears to be a large number of parameters required to specify any case of a sinusoidally time-dependent boundary layer and larval suspension and settling. These will be examined by dimensional analysis to reveal fundamental non-dimensional parameters so we can examine the behavior of the model and its sensitivity to this simplified non-dimensional parameter set.

The dimensional quantities are: z, t, $u(z, t)$, $v(z, t)$, $c(z, t)$, $u_*(t)$, u_h, u_{*max}, T, h, z_o, C_{total}, w_f, w_s, $\bar{k}_e(z, t)$, $\epsilon(z, t)$, $A_v(z, t)$, ρ, ν, f. Some are either fixed (density of water, Coriolis) or fully specified internal to the model ($\bar{k}_e(z, t)$, $\epsilon(z, t)$, $A_v(z, t)$). Most are

predicted by the model when all external forcing is given (u, v, c, u_* as functions of z and t). The variables which are externally specified are: u_h, u_{*max}, T, h, z_o, C_{total}, w_f, w_s.

This list has been divided up between externally specified parameters and those variables which are predicted by the equations of motion and suspension. There are several choices to make which affect the way we specify the model. For instance, the outer velocity field, u_h, could be found given the near bed stress, u_{*max}, or vice-versa. The near-bed stress will be specified because it is less affected by bed roughness changes and more closely connected to the strength of external forcing as given by an imposed external pressure gradient.

The momentum field can be fully non-dimensionalized by specification of the four variables u_{*max}, T, h, z_o. The concentration field and the bottom boundary condition are specified with the addition of C_{total}, w_f, w_s. These in turn may be combined to provide the non-dimensional controlling parameters:

$$h/z_o$$

$$w_f/u_{*max}$$

$$\frac{u_{*max}T}{h}\left[\frac{\delta_{bl}}{h} = \frac{\kappa u_* T/2\pi}{h}\right]$$

$$w_s/w_f.$$

The model gives all other variables as functions of these parameters and the independent time and space parameters, t/T and z/h (or z/z_o).

By specifying the model with the four parameters, h/z_o, w_f/u_{*max}, $u_{*max}\,T/h$, and w_s/w_f, we can examine many apparently different field conditions in a unified context. We chose these four parameters because each has an easily identifiable physical meaning. They correspond to relative roughness, Rouse number, depth limitation and a ratio of settlement flux to advective flux. At times one might want to consider different non-dimensional parameters such as w_fT/h or w_s/u_{*max}. These are not new independent parameters. They can be formed from the above set of four parameters and do not define additional different physical situations.

• *h/z_o, Relative roughness*

The relative roughness, h/z_o, is the ratio of the flow Reynolds number (u_*h/ν) to the roughness Reynolds number (u_*z_o/ν). In most field situations the relative roughness is large, i.e., $> 10^4$. Kinetic energy closure requires large Reynolds number flow with a hydrodynamically rough bed described by constant z_o. Therefore the model does allow small values of h/z_o to be investigated. On the other hand, variations in h/z_o do not affect model results in the limit of large h/z_o.

• δ_{bl}/h, *Boundary layer depth/Full depth*

The height of an oscillating turbulent boundary layer will be determined by the turbulent strength and the period of the oscillation; $\delta_{bl} = \alpha u_{*max} T/2\pi$ where α is a constant of order unity. The factor of 2π is included for consistency with commonly accepted terminology where radian frequency is used. The exact value of α is set by the definition of the top of a boundary layer. von Karman's constant, $\kappa = 0.4 = \alpha$, is often used in wave boundary layer studies (Grant and Madsen, 1986). We will use $\alpha = \kappa$. The parameter δ_{bl}/h is the ratio of boundary layer depth to total depth. If δ_{bl}/h is less than one then the depth of the water column is greater than the boundary layer depth and the turbulence generated near the bed will not communicate with the surface. On the other hand if δ_{bl}/h is greater than one the boundary layer is said to be depth limited and turbulence will be able to suspend material all the way to the surface. In an oscillatory flow where the parameter δ_{bl}/h is approximately one, the boundary layer will interact with the surface at maximum flow and not at minimum flow. These three cases will be seen to be important classifications of the behavior of the system.

• $w_f/\kappa u_{*max}$, Rouse Number

The steady state profile of larvae in suspension using a linear eddy diffusivity (as is appropriate near the bed) and uniform fall velocity has the solution of the Rouse profile (the concentration is known at a level z_1):

$$C(z) = C(z_1)(z_1/z)^{w_f/\kappa u_*}. \tag{19}$$

The exponent $w_f/\kappa u_*$ is known as the Rouse parameter and is a measure of the relative strength of downward flux due to fall velocity versus the upward turbulent suspension flux. A smaller Rouse number describes a more uniformly mixed profile, while a large Rouse number characterizes larvae of large fall velocity which remain close to the bed.

• w_s/w_f, *Settlement velocity to fall velocity*

There are three mechanisms of larval movement in this model. The advective fall flux, $w_f C$, the diffusive flux, $A_v\, \partial C/\partial z$ and the bed settlement flux, $w_s C$. At steady state, with zero settlement, the advective flux and diffusive flux balance and result in the Rouse profile. However when settlement is allowed the fluxes are out of balance and the ratio of settlement flux to either advective flux or diffusive flux becomes important. Either w_s/u_{*max} or w_s/w_f may be chosen as the parameter to describe these ratios. The combination of one of these and the fundamental parameter $w_f/\kappa u_{*max}$ provides the other.

Another useful nondimensional parameter is the ratio of the distance a larva can fall in one cycle to the total depth, $w_f T/h$. This is analogous to the turbulent

boundary layer depth limitation parameter. (In fact it is the product of δ_{bl}/h and w_f/u_{*max} and therefore not an additional independent parameter). The time dependence of larvae adjusting to changes in turbulent intensity will be described by this number. If $w_f T/h$ is large then larvae may possibly traverse the entire water column and drop out within one cycle. If $w_f T/h$ is small then there may be little time dependence in the concentration profile shape.

Table 1 lists some parameter combinations which are possible in nature and their non-dimensional parameters. The model parameters of the figures are listed in this table. Some other combinations of parameters are not physically realizable or important in the ocean. For instance values of u_{*max} fall mainly in the range of 0.5 – 5.0 cm/s and in shallow waters there is a spectral gap between tidal forcing and wind-wave forcing with periods of 5 to 20 seconds. Intermediate frequencies such as internal waves might be considered but we direct our attention to the tidal and wind-wave cases.

6. Results

An important hydrodynamic control of larval settlement will occur through the supply of larvae to the region below z_c. We examine this control by fixing the settlement flux at zero. Thus the total load of larvae in suspension is constant for these cases, and larvae move up and down through the forcing period. A variable describing the proportion of larvae found close enough to the bed to interact with it is

$$\tilde{C}_{z_c} = \frac{\int_{z_o}^{z_c} C(z)\,dz}{\int_{z_o}^{h} C(z)\,dz}. \tag{20}$$

This ratio defines the relative pool of potential settlers, and it varies from 1.0 for large z_c/h to zero for $z_c = z_o$.

The model cases below are forced by a single sinusoidal frequency. This simulates tidal flow in a channel or uniform shelf, or for high frequencies it simulates a monochromatic wind-wave field. Figure 4 shows the proportion of all larvae found below z_c, for both constant and variable z_c (Eq. 17), as the boundary layer oscillates through one period (Table 1, row 8). When the stress is high, at the beginning, middle and end, most of the larvae are suspended higher than z_c and $\tilde{C}_{z_c}$ is small. As the stress decreases through the ebbing current the near bed larval load increases. The maximum lags the time of lowest stress slightly because larvae are falling toward the bottom and still accumulating near the bed even after the stress has begun to increase.

The constant formulation for z_c was chosen to be three times the diameter of the grain size of particles comprising the bed, which we take to represent the approxi-

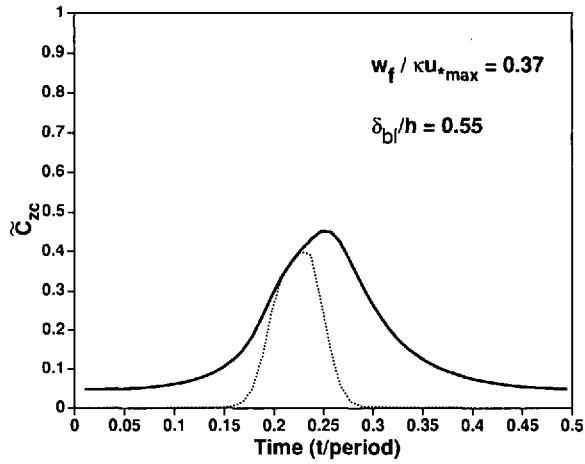

Figure 4. $\tilde{C}_{z_c}$ (the proportion of larvae below the level z_c) as a function of time. $z_c = 90\, z_o$: solid line. $z_c = 40\, w_f \nu / u_*^2$: dashed line.

mate scale of a "typical" larvae. For the variable $z_c = 40\, w_f \nu / u_*^2$, the layer thickness varies inversely with bottom stress, approaches maximum thickness during low stress and thins considerably when the stress is high. There is a greater change in proportion of larvae below z_c throughout the tidal cycle in comparison to the constant z_c case. In both cases, it is clear that the pool of larvae available for settlement is substantially greater at and near slack water than when currents are strong.

The four nondimensional parameters h/z_o, $w_f/\kappa u_{*max}$, δ_{bl}/h, and w_s/w_f, interact with one another to provide a rich set of cases which will be presented in forms similar to Figure 4. For these cases the relative roughness number is large and constant. Small Reynolds number flows violate assumptions of the TKE modeling method. Another non-dimensional ratio could be considered, namely the ratio of z_c/h or z_c/δ_{bl}. We simplify the evaluation of the nondimensional parameters by considering only the case of fixed z_c and therefore holding constant the ratio of z_c to full depth, h. A zero fall-velocity, fully mixed profile, would give $\tilde{C}_{z_c}$ equal to z_c/h, which could be a misleading artifact when z_c is varied.

Before considering the effects of settlement, the purely hydrodynamic control of larval supply to the bed will be examined through variation of the two parameters $w_f/\kappa u_{*max}$ and δ_{bl}/h. The temporal variability and the magnitude of $\tilde{C}_{z_c}$ will depend on the thickness of the turbulent boundary layer and upon the thickness of the larval-containing layer. $\tilde{C}_{z_c}$ will be decreased by thicker turbulent boundary layers, $u_{*max}T/2\pi$ (or δ_{bl}/h), or thinner larval-containing layers, and increased by larger w_f (or $w_f/\kappa u_{*max}$). Figure 5 examines these effects on $\tilde{C}_{z_c}$ for a range of $w_f/\kappa u_{*max}$ and δ_{bl}/h which might be found in tidal flows. The range of these parameters in nature

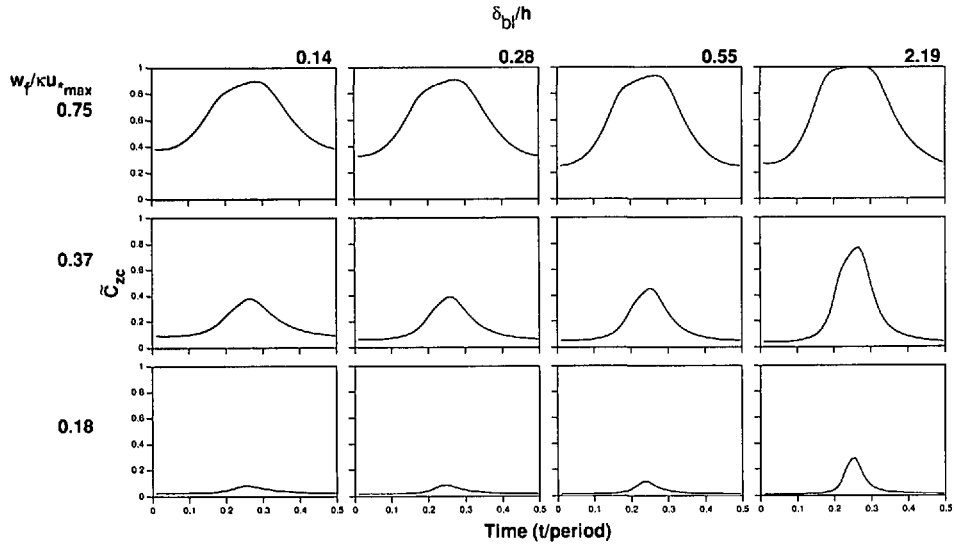

Figure 5. Each plot in this series shows the dependence of $\tilde{C}_{z_c}$ on phase of tide. The two parameters $w_f/\kappa u_{*max}$ and δ_{bl}/h are varied among figures. There is a strong dependence of the near bottom concentration profile on $w_f/\kappa u_{*max}$, and a weak dependence on δ_{bl}/h. The first column of 3 plots should be cross-referenced to rows 1–3 in Table 1. The second column of 3 plots to rows 4–6 in Table 1, etc.

may be larger than shown in this figure. But, as the figures show, their effects quickly reach asymptotic behavior.

• δ_{bl}/h

A boundary layer is not depth limited when the thickness of the layer containing significant turbulent kinetic energy is less than the water column height. When δ_{bl}/h is less than 1.0 the total depth is large enough that the boundary layer does not interact with the surface and any additional increase in h will not affect the near bed structure. A depth limited boundary layer is one in which energy generated by shear stress at the bottom is found distributed throughout the water column. When $\delta_{bl}/h \geq 2.5$ the boundary layer is clearly depth limited and larvae are well mixed all the way to the surface. At times of maximum u_*, $(t/T = 0.0, 0.5)$ the larvae are mostly above z_c and $\tilde{C}_{z_c}$ is small. The increase of the amplitude of the peak in $\tilde{C}_{z_c}$ at slack water is complicated by the time dependence of the flow. For the time period of slack water $0.15 < t/T < 0.35$ the particles fall from above and fill the region below z_c, thereby increasing $\tilde{C}_{z_c}$. The amplitude of the peak in $\tilde{C}_{z_c}$ at slack water increases with δ_{bl}/h because, in an absolute sense, this period of slack water is longer when the boundary layer is depth limited. That is, for constant $w_f/\kappa u_{*max}$ and h, a larger δ_{bl}/h can only be

created by increasing T and thereby increasing the time of slack water. The peak of $\bar{C}_{z_c}$ increases because more time is available for larvae to fall below z_c at slack water.

• $w_f/\kappa u_{*max}$

The depth-limitation effects on temporal variation in $\bar{C}_{z_c}$ are small when compared with the variation achieved when $w_f/\kappa u_{*max}$ is varied (Fig. 5). When $w_f/\kappa u_{*max}$ is increased by only a factor of two the proportion of larvae below z_c grows substantially. This reflects changes in the height of the larvae containing layer (i.e., the region below which most larvae are contained) which is controlled by $w_f/\kappa u_{*max}$, as in the Rouse solution for suspended sediments. In the field this parameter can vary over several orders of magnitude in part due to larval swimming behaviors. But, as Figure 5 shows, for all $w_f/\kappa u_{*max} < 0.10$ the larvae are well mixed above z_c and for all $w_f/\kappa u_{*max} > 1.0$ the larvae are almost all below z_c. The range of $w_f/\kappa u_{*max}$ which spans between the asymptotic cases is only $0.1 < w_f/\kappa u_{*max} < 1.0$. Larvae may have large gravitational fall velocities but because they actively swim their effective fall velocity may be near zero. Alternatively swimming behavior may cause the effective fall velocity to be several times their inert downward fall velocity. However within a boundary layer which is actively mixed by a large u_{*max} the frequency of bed encounters by an individual larvae may be large even though the ratio $w_f/\kappa u_{*max}$ is small (Denny and Shibata, 1989).

Boundary layers forced by wind generated waves are much thinner than tidal boundary layers. The time scale is 5 to 20 seconds with $u_* \approx 0.005 - 0.050$ m/s. Wave generated flows are seldom depth limited boundary layers as they are only a few tens of centimeters thick, or three orders of magnitude thinner than tidal flows. Therefore we might expect rather different behavior. Figure 6 demonstrates that even with large fall velocities the larvae remain at constant levels above the bed over a period of oscillation. Within one wave period a larvae may fall only a few centimeters each decelerating phase. The larvae fall even less because the turbulent kinetic energy responsible for resuspension is always relatively high near the bed. Therefore the larvae remain near a steady state level above the bed, well mixed throughout the boundary layer, but confined to the thin region where turbulent energy is maintained. The ratio of thickness of the boundary layer to z_c becomes important when it is small ($\approx 1 - 100$) as in these cases. Greater than fifty percent of all larvae occur below $90\, z_o$, (Fig. 6). In this figure we have sampled smaller values of z_c to highlight the weak temporal dependence of $\bar{C}_{z_c}$. The only time dependence is shown very near the bed over distances the particles can traverse within one cycle. This distance is less than $90\, z_o$, smaller than the size of larvae. The role of time dependence in wind generated wave boundary layers will not be expressed in changing concentration near the bed. But the temporal variability of near bed stress will be large.

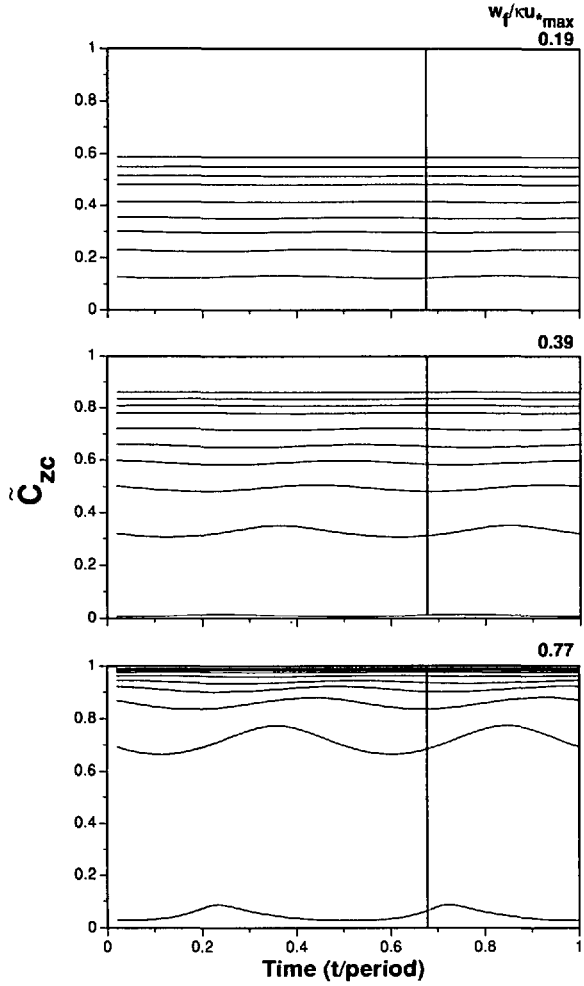

Figure 6. The dependence of $\bar{C}_{z_c}$ on time during a 20 s oscillation. The three plots are for three values of $w_f/\kappa u_{*max}$, as described in rows 13–15 in Table 1. Within each plot the series of curves are for $z_c = [z_o, 10\,z_o, 20\,z_o, \ldots 90\,z_o]$. Most of the larvae reside quite close to the bed. Because the magnitude of the energy remains relatively high throughout a cycle, there is little time structure.

• *w_s/w_f Settlement cases*

The zero settlement flux examples of Figures 4 and 5 indicate that for tidal flows most larvae are available for settlement for a short period at slack tide, and that considerably fewer are available when the flow is strong. Moreover, the slack period is also when the stress will fall below any defined τ_c for larval settlement. We therefore expect that settlement will occur primarily or only during this short time interval in tidally oscillating flows.

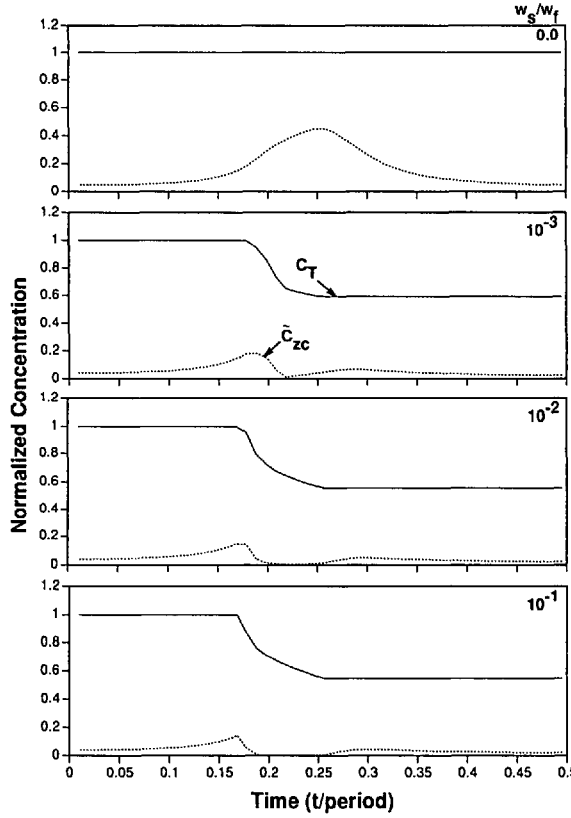

Figure 7. The effect of settlement on total larvae in suspension (C_T solid line) and near-bottom concentration ($\tilde{C}_{z_c}$ dashed line) for four values of $w_s/w_f = 0,10^{-3},10^{-2},10^{-1}$. The settlement flux is zero unless $\tau < \tau_c = 0.1\tau_{max}$, between times 0.17 and 0.29. The total larval load drops when the stress is below critical. Larvae are removed from the lowest strata and replaced by fall velocity or turbulent diffusion from above. When w_s is large the larvae do not fall fast enough to keep the concentration near the bed high and total settlement becomes independent of w_s/w_f.

We now consider a series of non-zero flux cases which will demonstrate the relative importance of boundary processes and larval supply from the water column to the bottom to settlement rates. The boundary processes which control larval settlement, which are parameterized by w_s, include lift and drag forces on larvae and behavioral responses to the substratum.

In the following cases critical stress (above which settlement is set to zero) was set to be 10% of maximum stress (Table 1, rows 16–18). The cases in which settlement is allowed are not steady state. Therefore the initial conditions will establish part of the solution. By starting with a steady state Rouse profile at time zero, and allowing the settlement flux to occur across nine periods, a nearly periodic solution is approached. In Figure 7 we show total concentrations of larvae in suspension (per unit area of bottom) and the proportion below z_c (for $z_c = 90\ z_o$) on the tenth cycle, non-

dimensionalized by the total concentration in suspension at the beginning of the cycle. By this time the initial transients from time zero have decayed and each successive nondimensional cycle is spatially and temporally similar, differing only by the concentration at the beginning of each cycle.

Figure 7 shows the effect on near bed concentration when settlement velocity is varied over several orders of magnitude. The parameter w_s/w_f is used to scale these examples. When w_s/w_f is small the flux out of the bottom is limited by w_s and there is a continuous slow drop in total concentration when τ is less than τ_c. As w_s/w_f is increased the concentration of particles near the bed decreases quickly while τ is less than τ_c. The total concentration drops rapidly as the near bed layer is depleted. Thereafter the drop in total concentration is limited by the flux from above the bed to the near bed region within z_c. Because the settlement flux becomes limited by the fall velocity and turbulent diffusive flux above the bed, the near bed boundary condition no longer controls settlement flux. For this case it appears that when w_s/w_f is greater than 10^{-2} it is no longer a controlling factor. The critical value of w_s/w_f is also dependent on the parameter $w_f/\kappa u_{*max}$. For large $w_f/\kappa u_{*max}$ fall velocity dominates the flux toward the bed. For small $w_f/\kappa u_{*max}$ turbulent diffusive flux will be more important and the flux limitation will be described by the value of $w_s/\kappa u_{*max}$.

Figure 8 shows the balance of advective and turbulent diffusive fluxes at the height of z_c and the settlement flux at the bed. Before and after settlement the advective and diffusive fluxes are large with only a small difference accounting for the changes in $\tilde{C}_{z_c}$. During the settlement period the magnitude of the advective and turbulent diffusive fluxes drops quickly with the drop in near bed larval concentration and u_*. When $w_s/w_f \geq 10^{-2}$ the settlement flux is limited by advective flux, i.e. the two are nearly in balance, and the turbulent diffusive flux approaches zero. Turbulent diffusive flux does not appear to be a limiting quantity. The relative strength of the advective flux to diffusive flux, w_f/u_{*max}, will establish the depth of the concentration profile prior to a settlement period while the ratio w_s/w_f will establish whether the flux will be limited by settlement velocity or advective velocity.

7. Discussion

The behavioral response of larvae to the substratum, driven by the composition of the bed as well as by the degree of larval competence to settle, will determine whether near-bed or water-column processes govern the net settlement. The model indicates that net larval settlement will be governed by the settlement velocity (w_s) when it is small, relative to the larval fall velocity (w_f). For this case, both the settlement velocity and settlement flux will be low, and net settlement will be independent of larval advection and mixing in the water column. In contrast, at higher p, the settlement flux will be governed by the supply of larvae from higher in the water column to the near-bottom region. The model indicates that hydrodynamic boundary processes may be important to settlement only when the probability of accepting the substratum (per unit time) is comparatively high.

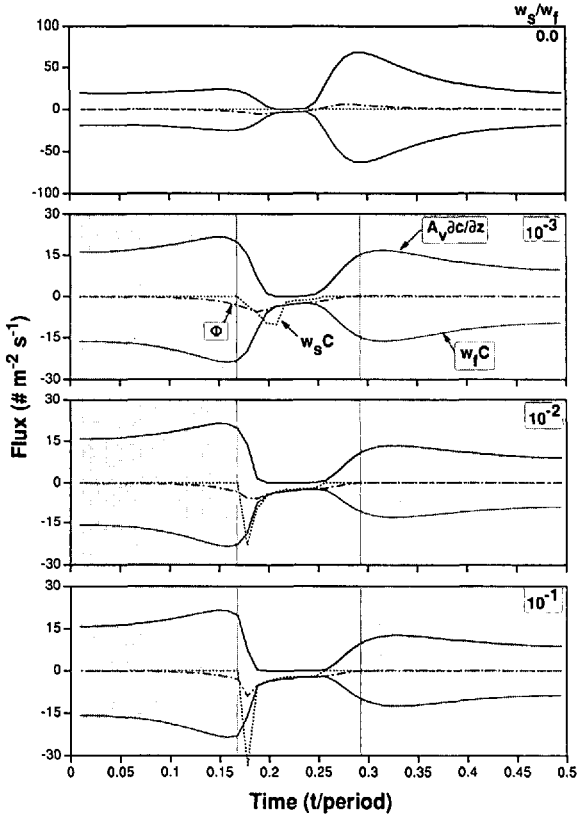

Figure 8. Near-bed fluxes for cases shown in Figure 7. Settlement flux at the bed, $w_s C(z_o)$, (dashed line). Advective flux at the level of z_c, $w_f C(z_c)$, (negative solid line). Turbulent diffusive flux at the level of z_c, $A_v\,(\partial C/\partial z)|_{z=z_c}$, (positive solid line). Total flux, Φ, at the level of z_c, (dash-dot line). The shaded areas indicate periods of excess bed stress when $w_s = 0$.

The Rouse parameter ($w_f/\kappa u_*$) describes the main hydrodynamic control of larval settlement. It determines the distribution of larvae throughout the water column, ranging from well mixed for small Rouse parameters, to near-bed concentrated for large Rouse parameters. Although it is termed a hydrodynamic control, it should be noted that the Rouse parameter is also subject to strong behavioral modification through the potential effect of larval swimming on w_f. Even a factor of two change in w_f by larval swimming can exert profound effects on the availability of larvae for settlement (Fig. 5). Such changes in w_f are easily imposed by larvae on gravitational sinking speeds which typically range from 0.01 – 1 cm/s (e.g., Young and Chia, 1984; Butman, 1986).

The fluxes of larvae into the near bed larval interaction region of height z_c are schematically shown in Figure 3. Although the time rate of change of concentration within the z_c region is always small relative to the flux gradients, the number of larvae within the region is controlled by the relative importance of the flux terms (Fig. 8).

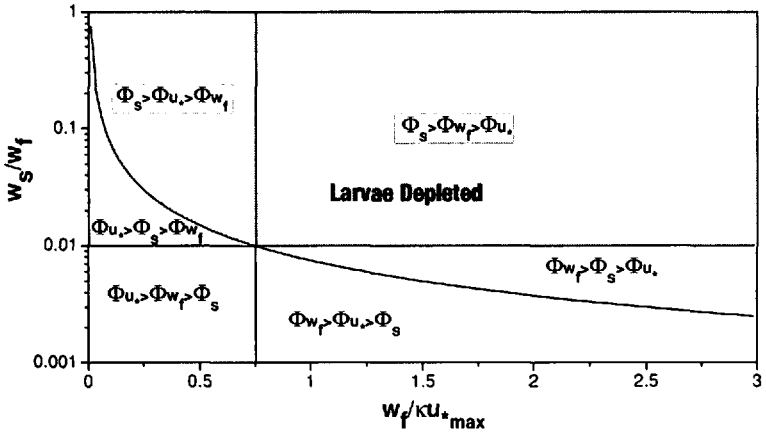

Figure 9. The interaction of settlement flux, Φ_S, fall velocity flux, Φ_{w_f} and diffusive flux, Φ_{u_*}, are described by the ratios w_s/w_f and $w_f/\kappa u_{*max}$. The lines demark sections where the relative effect of one flux dominates over the other two. Within a distance z_c of the bottom, depletion of larvae occurs only in the sections where Φ_S is the largest of the three fluxes (hatched area). Otherwise the settlement is small and the source from above, either through Φ_{w_f} or Φ_{u_*}, is enough to prevent depletion within the z_c region.

When settlement flux, Φ_S, is largest, advection and diffusion, Φ_{w_f} and Φ_{u_*}, of larvae from above do not keep up with settlement and the region becomes depleted of larvae. When Φ_S is small, one or the other of the source fluxes will dominate, maintaining a concentration of larvae within the region. When Φ_{u_*} is the strongest flux the profile is well mixed throughout the boundary layer, including the region within z_c. On the other hand, when Φ_{w_f} is largest the profile increases towards the bed as a Rouse profile.

The relative importance of the flux terms can be plotted on a single graph of w_s/w_f versus $w_f/\kappa u_{*max}$ (Fig. 9). From our model results we have found that the balance of settling flux to fall flux is approximately achieved when $w_s/w_f \approx 10^{-2}$ (Figs. 7 and 8). The separation of Rouse-type profiles from well mixed profiles occurs at $w_f/\kappa u_{*max} \approx 0.75$ (Fig. 5). These lines are plotted along with the line representing the balance of settling flux to diffusive flux, $w_s/w_f \times w_f/\kappa u_{*max} \approx 0.75 \times 10^{-2}$. The relative importance of flux contributions within the different sections is indicated. Note that on this graph the depleted larvae cases occur in only two sections, where $\Phi_S > \Phi_{u_*} > \Phi_{w_f}$, the well mixed case, and $\Phi_S > \Phi_{w_f} > \Phi_{u_*}$, the Rouse-type case. The two sections at the bottom of the graph where Φ_S is minimum are the zero or very small settlement "steady state" cases. The other two sections wherein Φ_S is greater than Φ_{w_f} (or Φ_{u_*}) but is less than the other flux, correspond to conditions where settlement is maintained by diffusive flux, $\Phi_{u_*} > \Phi_S > \Phi_{w_f}$ (or fed by the fall flux, $\Phi_{w_f} > \Phi_S > \Phi_{u_*}$).

Larval behavior can change net settlement by affecting either w_f or w_s. Changes in

w_s will only affect the settlement flux in regions of the graph which are amply supplied with larvae, the non-depleted regions. And similarly, changes of w_f will only affect settlement flux when Φ_S dominates. Simply stated the net settlement depends only upon the limiting flux term. This graph suggests that experimental evidence of larval control over net settlement will be found only in regions limited by fluxes that can be affected by larval behavior. In the sections where Φ_{w_f} is limiting, $w_f/\kappa u_{*max} < 0.75$ and $w_s/w_f > 0.01$, larval swimming behavior may affect net settlement. Larval settlement behavior may affect net settlement only in the sections where Φ_S is limiting, $\Phi_{w_f} > \Phi_{u_*} > \Phi_S$ and $\Phi_{u_*} > \Phi_{w_f} > \Phi_S$ (where w_S/w_f is the smaller of 0.01 or $w_s/w_f < 0.75 \times 10^{-2}\kappa u_*/w_f$). These sections of Figure 9 define the ranges of the parameters w_s/w_f and $w_f/\kappa u_{*max}$ wherein larval control of net settlement can be observed.

Larval swimming and responses to the substratum may have dominant effects on the settlement rate. These behaviors must be studied and quantified accurately if we are ever to discern the relative influences of behavior and hydrodynamics on settlement. In particular, we do not know even approximate ranges of the parameter p, which are needed before we know whether it is important to focus on the boundary (loss) or the internal flow (larval supply) in predicting settlement rates. This model has helped to point out that p or w_s can be studied independently of a complicated turbulent boundary layer.

We have so far made the simplifying assumptions that w_f is independent of time and depth, and that p exhibits a simple shear dependence. Whereas these terms may be impacted significantly, if not dominated, by larval behavior, there is little doubt that nature will prove to be more complex. For example larval swimming may be light and pressure (and therefore depth) dependent, and may be sensitive to turbulence or Reynolds stress (Jonsson *et al.,* 1991; Pawlik *et al.,* 1991). Attachment probability, p, may exhibit a far more complex dependence on u_* than that assumed herein, due to influences of lift and drag forces on larvae exploring the bottom (cf., Eckman *et al.,* 1990). These shear and depth dependent behaviors are poorly understood, yet they may greatly impact predictions of larval settlement rate.

The model predicts that there may be substantial temporal variability in rates of settlement over tidal time scales (Figs. 4 and 5). Most of the settlement may occur at and near periods of slack tide, and comparatively little during periods of strong flow. If it is realized in nature, this prediction could help to explain oft-noted spatial heterogeneity in benthic recruitment, as settlement may be most intense where a patch of planktonic larvae are located when the tide goes slack. However, it is possible that larval behaviors, such as flow-dependent swimming responses, may mask or override this predicted pattern of settlement (Pawlik *et al.,* 1991).

Our examples all used a simple sinusoidal outer velocity forcing. Other time dependencies could be studied. Steady state cases are simply profile solutions which are asymptotically approached for very large $\kappa u_* T/2\pi h = \delta_{bl}/h$ cases. Another class

of time dependence not discussed here is that of rotary currents. The current speed need not ever pass through zero and thus u_*, k_e and therefore A_v may not vary strongly in time. Under these conditions the suspended larval concentration approaches the steady state solution. In nature we expect to encounter a variety of time scales which will interact to provide a more complicated time dependence. For instance, the spring-neap tidal cycle may intensify settlement rates on a bi-weekly schedule or storms may interrupt the simple tidal forcing and settlement patterns. These cases may be important in some settings. But the conclusions gleaned from the sinusoidal forcing cases will still hold when the dominant time scale of interest can be identified.

The continuum one dimensional model of larval suspension is best used to give gross availability to the lowest layer. Although the momentum and energy equations are well posed and naturally require resolution near z_o of fractions of z_o, the boundary conditions on larval suspension near the bed seem to behave unrealistically. The no-flux condition at the bed results in a strong gradient of concentration at heights of order a few z_o and always a large concentration in the lowest resolved depth stratum. A larvae of length $\approx 30\, z_o$ cannot increase in concentration across length scales of a few z_o. There is no abnormal effect of these artificial, near-bed conditions on the outer concentration profile nor on the flux toward the bed. But they point out a weakness in the conceptual model. Namely the extrapolation of steady state conditions to settlement conditions near the bed yields an unrealistic view of large larval gradients and rapid flux. However the large concentration very near the bed is only a transient phase found before and just after settlement flux is started. Because we are using bed flux conditions which are specific rates (i.e. a settlement velocity times the near-bed concentration) the boundary condition is affected by the realism of the concentration near the bed.

A computational approach which avoids continuum concentration problems is to use Lagrangian particle tracking methods (Gidhagen *et al.*, 1988; Thomson, 1984). Particles representing individual larvae are released into the turbulent flow defined by the TKE model and allowed to advect and "random walk" through the water column. The larvae will be allowed to interact with the bed when they are within z_c just as in our model. But because the larvae can be given finite size they will not "overconcentrate" at distances too close to the bed. More realistic conditions near the bed should result.

8. Concluding remarks

A model of suspended larval concentration was used to demonstrate the relative effects of hydrodynamic and behavioral controls on settlement. A relatively simple TKE closure method provided a fully time dependent profile of turbulent eddy diffusivity. Non-dimensionalization yielded four parameters which describe most of the model cases: z_o/h, δ_{bl}/h, $w_f/\kappa u_{*max}$ and w_s/w_f. The range of effect for these

parameters is surprisingly narrow. The system quickly approaches asymptotic behavior outside the ranges demonstrated. From a purely hydrodynamic standpoint the Rouse parameter $w_f/\kappa u_{*max}$ had the strongest influence on availability of larvae to the bed for settlement. The settlement flux will be limited by w_s, which parameterizes settlement behavior near the bed, and by rate of supply of larvae from higher in the water column. The rate of supply will be the larger flux of either fall velocity flux or diffusion flux. The controlling parameter of settlement is thus the smaller of w_s/w_f or $w_s/\kappa u_{*max}$.

This methodology provides a framework in which we can work on the controls of larval settlement rates. Most of the unknown problems fall upon the parameter, w_s, and the probability of larvae selecting the bottom for settlement. Progress on the biologically complicated problem involved in estimating $w_s = pz_c$ must be made before we consider further dynamic interactions with time varying flow and variable bed roughness.

Acknowledgments. This research, which is part of the GLOBEC program, was supported by NSF Grant OCE-9016825.

APPENDIX A

Numerical treatment of the concentration equation

The equations are transformed from (z, t) coordinates to log-linear (ξ, t) coordinates, e.g., Davies *et al.* (1988), where

$$\xi = \frac{1}{\chi}\left\{\ln\left(\frac{z}{z_o}\right) + \left(\frac{z - z_o}{z_*}\right)\right\} \tag{A1}$$

and

$$\chi = \ln\left(\frac{h}{z_o}\right) + \left(\frac{h - z_o}{z_*}\right). \tag{A2}$$

Here h is the height of the model domain, z_o is the roughness length and z_* a stretching term in the coordinate transformation where $z_o < z_* < h$. Our numerical treatment of the momentum and energy equations follows the staggered formulation of Ozer *et al.* (1988) and Davies and Jones (1991). The details of the discretization of the concentration equation follow next. In log-linear coordinates, Eq. (1) is

$$\frac{\partial C}{\partial t} + \frac{1}{(\chi z_*)}\left(1 + \frac{z_*}{z(\xi)}\right)\frac{\partial (w_f C)}{\partial \xi} = \frac{1}{(\chi z_*)^2}\left(1 + \frac{z_*}{z(\xi)}\right)\frac{\partial}{\partial \xi}\left[\left(1 + \frac{z_*}{z(\xi)}\right)A_v \frac{\partial C}{\partial \xi}\right] \tag{A3}$$

and in discrete form

$$\frac{\delta_t C_k^n}{\Delta t} + \frac{\theta_{ad} r(\tilde{z}_k)}{2}\left[(w_f)_{k+1/2}^{n+1} C_{k+1}^{n+1} - (w_f)_{k-1/2}^{n+1} C_{k-1}^{n+1}\right] + (1-\theta_{ad})\frac{r(\tilde{z}_k)}{2}$$
$$\times \left[(w_f)_{k+1/2}^{n} C_{k+1}^{n} - (w_f)_{k-1/2}^{n} C_{k-1}^{n}\right] = \theta_{con} r(\tilde{z}_k) \qquad \text{(A4)}$$
$$\times \left[r(z_{k+1})(A_v)_{k+1/2}^{n+1}\delta_\xi C_k^{n+1} - r(z_k)(A_v)_{k-1/2}^{n+1}\delta_\xi C_{k-1}^{n+1}\right]$$
$$+ (1-\Theta_{con}) r(\tilde{z}_k)\left[r(z_{k+1})(A_v)_{k+1/2}^{n}\delta_\xi C_k^{n} - r(z_k)(A_v)_{k-1/2}^{n}\delta_\xi C_{k-1}^{n}\right]$$

where the only unknowns are the C^{n+1}'s. The δ_t and δ_ξ are forward difference operators in time and space respectively, e.g., $\delta_t C_k^n = C_k^{n+1} - C_k^n$. $r(\tilde{z}_k) = (\chi z_* \Delta\xi)^{-1} \times (1 + z_*/\tilde{z}_k)$ and analogously for $r(z_k)$ and $r(z_{k+1})$. The subscripts $k \pm \frac{1}{2}$ indicate averaging of the variable, e.g., $(w_f)_{k+1/2}^{n+1} = 0.5[(w_f)_{k+1}^{n+1} + (w_f)_k^{n+1}]$, where k is the spatial index and n the temporal index. The $\tilde{z}$ corresponds to locations where the concentration is evaluated and z without the tilde to the mesh locations where the velocity is evaluated ($\tilde{z}$ and z are staggered, Figure 1), and θ_{ad} and θ_{con} are weights between time n and $n+1$ such that the formulation is fully implicit if they are 1 and fully explicit if they are 0. Here we use $(\theta_{ad}, \theta_{con}) = (0.5, 1.0)$.

At the bottom we explicitly write an equation for the time rate of change of C as a function of the advective and turbulent flux from "above" and the settlement/resuspension flux from "below"

$$\frac{\partial C}{\partial t} = -\frac{1}{\delta z}\left[\Phi_{above} - \Phi_{below}\right] \qquad \text{(A5)}$$

where

$$\Phi_{above} = \left(w_f C - A_v \frac{\partial C}{\partial z}\right)_{z_o + \delta z} \qquad \text{(A6)}$$

and

$$\Phi_{below} = (w_s C + w_e C_{bed})\big|_{z_o}. \qquad \text{(A7)}$$

Here w_s is the settlement velocity, w_e is the erosion rate/velocity and C_{bed} is the concentration in the bed. In discrete form (A5) − (A7) at the bottom, $k = 1$, are

$$\frac{\delta_t C_1^n}{\Delta t} = -r(\tilde{z}_1)\left\{\frac{\theta_{ad}}{2}\left[(w_f)_{3/2}^{n+1} C_2^{n+1} + (w_f)_{1/2}^{n+1} C_1^{n+1}\right] - \theta_{con}\, r(z_1)(A_v)_{1/2}^{n+1}(C_2^{n+1} - C_1^{n+1})\right.$$
$$- \frac{w_s^{n+1}\theta_{ad}}{2}(3C_1^{n+1} - C_2^{n+1}) + \theta_{bed}\, w_e^{n+1} C_{bed}^{n+1} + \frac{(1-\theta_{ad})}{2}\left[(w_f)_{3/2}^{n} C_2^{n} + (w_f)_{1/2}^{n} C_1^{n}\right]$$
$$\left. - \theta_{con} r(z_1)(A_v)_{1/2}^{n}(C_2^{n} - C_1^{n}) - \frac{w_s^{n}\theta_{ad}}{2}(3C_1^{n} - C_2^{n}) + \theta_{bed} w_e^{n} C_{bed}^{n}\right. \qquad \text{(A8)}$$

where θ_{bed} is the weight between time n and $n + 1$. Note that w_f is staggered relative to C and hence $(w_f)_{3/2}$ interpolates onto C_2 and similarly for $(w_f)_{1/2}$ and C_1. The value of C at the bottom is approximated by $C_{\xi=0} \simeq (3C_1 - C_2)/2$. At the top we impose a condition analogous to (A5) and require zero flux, i.e., no particle source/sink at the top, $\phi_{above} = 0$, and ϕ_{below} is of the same form as (A6). The system of equations is set up in tri-diagonal form and solved with standard banded matrix solver.

APPENDIX B

The pressure gradient term

Knowing the value of the pressure gradient term

$$P = -\left(\frac{1}{\rho}\right)\frac{\partial P}{\partial x} - i\left(\frac{1}{\rho}\right)\frac{\partial P}{\partial y} \tag{B1}$$

solutions to (3) and (4) are obtained by requiring no stress at the top

$$A_v \frac{\partial u}{\partial z} = 0, \qquad A_v \frac{\partial v}{\partial z} = 0 \tag{B2}$$

and no slip at the bottom (Eq. 5). Since P is known it is imposed at each step as a known ("right-hand side") term. However, if P is not known *a priori* but we do know u_h and v_h (Eq. 6; the free-stream/geostrophic velocity components above the boundary layer), then we calculate P as part of the solution (Ozer *et al.,* 1988) as follows.

As above, we require no stress (B2) at the top, and no slip at the bottom and write the resulting system of equations in discrete matrix form

$$\mathbf{A}^n\mathbf{w}^{n+1} = \mathbf{B}^n + \theta_p P^{n+1}\mathbf{I} \tag{B3}$$

where $\mathbf{w}\,(=u + iv, i = \sqrt{-1})$ is the vector of unknowns, i.e., at time $n + 1$; $\mathbf{I}$ is the unit vector; $\mathbf{A}$ is the left-hand-side matrix of known entries; $\mathbf{B}$ the known right-hand-side vector; and θ_p is the temporal weighting of the pressure terms which we treated fully implicitly, i.e., $\theta_p = 1$. Redefining $\mathbf{w}$ as

$$\mathbf{w}^{n+1} = \mathbf{w}_*^{n+1} + \theta_p P^{n+1}\boldsymbol{\lambda}^{n+1} \tag{B4}$$

we can rewrite (B3)

$$\mathbf{A}^n(\mathbf{w}_*^{n+1} + \theta_p P^{n+1}\boldsymbol{\lambda}^{n+1}) = \mathbf{B}^n + \theta_p P^{n+1}\mathbf{I} \tag{B5}$$

where $\mathbf{w}_*^{n+1}$ and $\boldsymbol{\lambda}^{n+1}$ are solutions to

$$\mathbf{A}^n\mathbf{w}_*^{n+1} = \mathbf{B}^n \tag{B6}$$

$$\mathbf{A}^n\boldsymbol{\lambda}^{n+1} = \mathbf{I} \tag{B7}$$

The unknown pressure gradient term is obtained using the known velocity $w_{kl}{}^{n+1}$ at

node kl (Eq. 6) at the top of the model domain

$$w_{kl}^{n+1} = u_h^{n+1} + iv_h^{n+1} = w_{*kl}^{n+1} + \theta_p P^{n+1} \lambda_{kl}^{n+1} \tag{B8}$$

or

$$P^{n+1} = \frac{1}{\theta_p \lambda_{kl}^{n+1}} (w_{kl}^{n+1} - w_{*kl}^{n+1}) \tag{B9}$$

where $\mathbf{w}_*^{n+1}$ and $\boldsymbol{\lambda}^{n+1}$ are known from the solutions to (B6) and (B7). The remaining $\mathbf{w}^{n+1}$, for $k = k_2$ to $(kl - 1)$ are obtained from

$$\mathbf{w}_k^{n+1} = \mathbf{w}_{*k}^{n+1} + \theta_p P^{n+1} \boldsymbol{\lambda}_k^{n+1} \tag{B10}$$

Table of Symbols

Quantity	Dimension	Description
A_v	l^2t^{-1}	Eddy diffusivity
C	$\#l^{-3}$	Concentration of larvae (number/volume)
C_a		TKE closure constant
C_e		TKE closure constant
C_ϵ		TKE closure constant
$\tilde{C}_{z_c}$		Proportion of larvae within distance z_c of bed
C_d		Drag Coefficient
C_{bed}	$\#l^{-3}$	Concentration of larvae in bed
C_{total}	$\#l^{-2}$	Total initial number of larvae in suspension per area = $\int_{z_o}^{h} c(z,\ t = 0)\, dz$
f	t^{-1}	Coriolis frequency
h	l	Total Depth
k_b	l	Physical bed roughness scale
k_e	l^2t^{-2}	Turbulent kinetic energy
l, l_o	l	Mixing length and asymptotic value
N	$\#l^{-2}$	Number of larvae per area
p	t^{-1}	Probability of settlement per time
P	$ml^{-1}t^{-2}$	Pressure
t	t	Time
t_q	t	Quiet time between turbulent bursting
T	t	Period of oscillation
u, v	lt^{-1}	Velocity of flow in X, Y directions
u_h, v_h	lt^{-1}	Maximum outer velocity components
u_{*max}	lt^{-1}	Maximum shear stress at the bed
u_*	lt^{-1}	Shear stress velocity scale
$\mathbf{w}$	lt^{-1}	Complex velocity
w_e	lt^{-1}	Erosion velocity
w_f	lt^{-1}	Fall velocity of particles
w_s	lt^{-1}	Settlement velocity
z	l	Height above the bed
z_c	l	Interaction distance of larvae with bed
z_o	l	Roughness length scale of sea bed ($z_o = k_b/30$)

Table of Symbols Continued

Quantity	Dimension	Description
z_*	l	Log-linear transformation height
$Z_{\delta_{bl}}$	l	Height of linear drag law
γ		TKE closure constant
δ_{bl}	l	Depth of turbulent boundary layer
ϵ	l^2t^{-3}	Turbulent kinetic energy dissipation
κ		von Karman's constant = 0.4
ν	l^2t^{-1}	Molecular diffusivity
ρ	ml^{-3}	Density of water
τ_b	$ml^{-1}t^{-2}$	Bed shear stress, $\rho u_*^2 = \tau_b$
τ_c	$ml^{-1}t^{-2}$	Critical stress threshold for deposition
Φ	$\#l^{-2}s^{-1}$	Flux of larvae
Φ_S	$\#l^{-2}s^{-1}$	Bed settlement flux
Φ_{u_*}	$\#l^{-2}s^{-1}$	Diffusive flux
Φ_{w_f}	$\#l^{-2}s^{-1}$	Advective fall velocity flux

REFERENCES

Bandyopadhyay, P. R. 1987. Rough-wall turbulent boundary layers in the transition regime. J. Fluid Mech., *180,* 231–266.

Blackadar, A. K. 1962. The vertical distribution of wind and turbulent exchange in a neutral atmosphere. J. Geophys. Res., *67,* 3095–3120.

Bradshaw, P., D. H. Ferriss and N. P. Atwell. 1967. Calculation of boundary-layer development using the turbulent energy equation. J. Fluid Mech., *C29,* 593–616.

Butman, C. A. 1986. Larval settlement of soft-sediment invertebrates: some predictions based on an analysis of near-bottom velocity profiles, *in* Marine Interfaces Ecohydrodynamics, Oceanography Series, *42,* J. C. J. Nihoul, ed., Elsevier, 487–513.

Butman, C. A., J. P. Grassle and C. M. Webb. 1988. Substrate choices made by marine larvae settling in still water and in a flume flow. Nature, *333,* 771–773.

Cantwell, B. J. 1981. Organized motion in turbulent flow. Ann. Rev. Fluid Mech., *13,* 457–515.

Connell, J. H. and R. O. Slatyer. 1977. Mechanisms of succession in natural communities and their role in community stability and organization. Amer. Natur., *111,* 1119–1144.

Crisp, D. J. 1984. Overview of research on marine invertebrate larvae, 1940–1980, *in* Marine Biodeterioration: an Interdisciplinary Study, J. D. Costlow and R. C. Tipper, eds., Naval Inst. Press, 103–126.

Dade, W. B., A. R. M. Nowell and P. A. Jumars. 1988. Mass arrival mechanisms and clay deposition at the seafloor, *in* Microstructure of Fine-Grained Sediments From Mud to Shale. R. H. Bennett, W. R. Bryant and M. H. Hulbert, eds., Springer Verlag, Heidelberg, 161–164.

Davies, A. G. 1986. A numerical model of the wave boundary. Cont. Shelf Res., *6,* 715–739.

Davies, A. G., R. L. Soulsby and H. L. King. 1988. A numerical model of the combined wave and current bottom boundary layer. J. Geophys. Res. *93,* 491–508.

Davies, A. M. and J. E. Jones. 1991. On the numerical solution of the turbulence entergy equations for wave and tidal flows. Int. J. Num. Methods Fluids, *12,* 17–41.

Denny, M. W. and M. F. Shibata. 1989. Consequences of surf-zone turbulence for settlement and external fertilization. Amer. Natur., *134,* 859–889.

Eckman, J. E. 1983. Hydrodynamic processes affecting benthic recruitment. Limnol. Oceanogr., *28,* 241–257.

—— 1987. The role of hydrodynamics in recruitment, growth and survival of *Argopecten irradians* (L.) and *Anomia simplex* (D'Orbigny) within eelgrass meadows. J. Exp. Mar. Biol. Ecol., *106,* 165–192.

—— 1990. A model of passive settlement by planktonic larvae onto bottoms of differing roughness. Limnol. Oceanogr., *35,* 887–901.

Eckman, J. E., W. B. Savidge and T. F. Gross. 1990. Relationship between duration of cyprid attachment and drag forces associated with detachment of *Balanus amphitrite* cyprids. Mar. Biol. *107,* 111–118.

Ekman, S. 1967. Zoogeography of the Sea, 2nd ed. Sidgwick and Jackson, 417 pp.

Fairweather, P. G. 1988. Consequences of supply-side ecology: manipulating the recruitment of intertidal barnacles affects the intensity of predation upon them. Biol. Bull., *175,* 349–354.

Gidhagen, L., L. Rahm and L. Nyberg. 1989. Lagrangian modelling of dispersion, sedimentation and resuspension processes in marine environments. Deut. Hydrog. Z., *42,* 249–270.

Grant, W. D. and O. S. Madsen. 1982. Moveable bed roughness in unsteady oscillatory flow. J. Geophys. Res., *87,* 409–481.

—— 1986. The continental-shelf bottom boundary layer. Ann. Rev. Fluid Mech., *18,* 265–305.

Gray, J. S. 1974. Animal-sediment relationships. Oceanogr. Mar. Biol. Ann. Rev., *12,* 223–261.

Grosberg, R. K. 1982. Intertidal zonation of barnacles: the influence of planktonic zonation of larvae on vertical distribution of adults. Ecology, *63,* 894–899.

Gross, T. F. and W. B. Dade. 1991. Suspended sediment storm modeling. Mar. Geol., *99,* 343–360.

Gross, T. F. and A. R. M. Nowell. 1990. Turbulent suspension of sediments in the deep sea. Phil. Trans. R. Soc. Lond., *A331,* 167–181.

Jackson, G. A. 1986. Interaction of physical and biological processes in the settlement of planktonic larvae. Bull. Mar. Sci., *39,* 202–212.

Jonsson, P. R., C. André and M. Lindegarth. 1991. Swimming behaviour of marine bivalve larvae in a flume boundary-layer flow: evidence for near-bottom confinement. Mar. Ecol. Prog. Ser., *79,* 67–76.

Keough, M. J. and B. J. Downes. 1982. Recruitment of marine invertebrates: the role of active larval choices and early mortality. Oecologia (Berl.), *54,* 348–352.

Meadows, P. S. and J. I. Campbell. 1972. Habitat selection by aquatic invertebrates. Adv. Mar. Biol., *10,* 271–382.

Middleton, G. V. and J. B. Southard. 1984. Mechanics of Sediment Movement, 2nd ed., Soc. Econ. Paleontol. Mineralog., Tulsa, Oklahoma, 401 pp.

Mofjeld, H. O. and J. W. Lavelle. 1984. Setting the length scale in a second-order closure model of the bottom boundary layer. J. Phys. Oceanogr., *14,* 833–839.

Nikuradse, J. 1933. Laws of flow in rough pipes. National Advisory Committee on Aeronautics, Technical Memorandum 1292 (English Translation), 62 pp.

Ozer, J., B. M. Jamart and S. Scory. 1988. One dimensional modelling of the turbulent bottom boundary layer, with application to the BSEX North Sea data set. MUMM's contribution to BSEX, Tech. Rep. No. TR08, 1st Draft, Mathematical Unit of the Mathematical Models of the North Sea and Scheldt Estuary, Belgium, 61 pp.

Paine, R. T. 1979. Disaster, catastrophe and local persistence of the sea palm *Postelsia palmaeformis.* Science, *205,* 685–687.

Pawlik, J. R., C. A. Butman and V. R. Starczak. 1991. Hydrodynamic facilitation of gregarious settlement of a reef-building tube worm. Science, *251,* 421–424.

Peterson, C. H. 1986. Enhancement of *Mercenaria mercenaria* densities in seagrass beds: is pattern fixed during settlement season or altered by subsequent differential survival? Limnol. Oceanogr., *31,* 200–205.

Pineda, J. 1991. Predictable upwelling and the shoreward transport of planktonic larvae by internal tidal bores. Science, *253,* 548–551.

Rodi, W. 1984. Turbulence Models and Their Application in Hydraulics: A State of the Art Review. 2nd rev. ed. The Netherlands: International Association for Hydraulic Research.

Roughgarden, J., S. Gaines and H. Possingham. 1988. Recruitment dynamics in complex life cycles. Science, *241,* 1460–1466.

Scheltema, R. S. 1974. Biological interactions determining larval settlement of marine invertebrates. Thalassia Jugosl., *10,* 263–296.

Shanks, A. L. 1986. Tidal periodicity in the daily settlement of intertidal barnacle larvae and an hypothesized mechanism for the cross-shelf transport of cyprids. Biol. Bull., *170,* 429–440.

Shanks, A. L. and W. G. Wright. 1987. Internal-wave-mediated shoreward transport of cyprids, megalopae and gammarids and correlated longshore differences in the settling rate of intertidal barnacles. J. Exp. Mar. Biol. Ecol., *114,* 1–14.

Sheng, Y. P. and W. Lick. 1979. The transport and resuspension of sediments in a shallow lake. J. Geophys. Res., *84,* 1809–1826.

Smith, J. D. 1977. Modeling of sediment transport on continental shelves, *in* The Sea, *6,* E. D. Goldberg *et al.,* eds., Wiley, New York, 539–57.

Smith, J. D. and S. R. McLean. 1977. Boundary layer adjustments to bottom topography and suspended sediment, *in* Bottom Turbulence, J. C. J. Nihoul, ed., Elsevier Scientific Publishing Co., Amsterdam, 123–151.

Soulsby, R. L. 1990. Tidal-current boundary layers, *in* The Sea, *9,* part A, B. LeMehaute and D. M. Hades, eds., J. Wiley and Sons Inc., New York, 523–566.

Summerson, H. C. and C. H. Peterson. 1984. Role of predation in organizing benthic communities of a temperate-zone seagrass bed. Mar. Ecol. Prog. Ser., *15,* 63–77.

Thomson, D. J. 1984. Random walk modeling of diffusion in inhomogeneous turbulence. Quart. J. R. Met. Soc., *110,* 1107–1120.

Wethey, D. S. 1986. Ranking of settlement cues by barnacle larvae: influence of surface contour. Bull. Mar. Sci., *39,* 393–400.

Wiberg, P. L. 1988. Mechanics of bedload sediment transport. J Sci. & Eng., *48,* 146.

Wiberg, P. L. and J. D. Smith. 1989. Model for calculating bed load transport of sediment. J. Hydraulic Engin., *115,* 101–123.

Wolanski, E. and W. M. Hamner. 1988. Topographically controlled fronts in the ocean and their biological influence. Science, *241,* 177–181.

Woodin, S. A. 1986. Settlement of Infauna: Larval Choice? Bull. Mar. Sci., *39,* 401–407.

Young, C. M. and F.-S. Chia. 1984. Microhabitat associated variability in survival and growth of subtidal ascidians during the first 21 days after settlement. Mar. Biol., *81,* 61–68.

Received: *Add* revised: *22 September, 1992.*